

Probing the phonon confinement in ultrasmall silicon nanocrystals reveals a size-dependent surface energy

Iain F. Crowe,^{1,a)} Matthew P. Halsall,¹ Oksana Hulko,² Andrew P. Knights,² Russell M. Gwilliam,³ Maciej Wojdak,⁴ and Anthony J. Kenyon⁴

¹Photon Science Institute and School of Electrical and Electronic Engineering, University of Manchester, Manchester M13 9PL, United Kingdom

²Department of Engineering Physics and the Centre for Emerging Device Technologies, McMaster University, Hamilton, Ontario L8S 4L7 Canada

³Surrey Ion Beam Centre, Advanced Technology Institute, University of Surrey, Guildford GU2 5XH, United Kingdom

⁴Department of Electronic and Electrical Engineering, University College London, London WC1E 7JE, United Kingdom

(Received 17 December 2010; accepted 12 March 2011; published online 22 April 2011)

We validate for the first time the phenomenological phonon confinement model (PCM) of H. Richter, Z. P. Wang, and L. Ley [Solid State Commun. **39**, 625 (1981)] for silicon nanostructures on the sub-3 nm length scale. By invoking a PCM that incorporates the measured size distribution, as determined from cross-sectional transmission electron microscopy (X-TEM) images, we are able to accurately replicate the measured Raman line shape, which gives physical meaning to its evolution with high temperature annealing and removes the uncertainty in determining the confining length scale. The ability of our model to explain the presence of a background scattering spectrum implies the existence of a secondary population of extremely small (sub-nm), amorphous silicon nanoclusters which are not visible in the X-TEM images. Furthermore, the inclusion of an additional fitting parameter, which takes into account the observed peak shift, can be explained by a size-dependent interfacial stress that is minimized by the nanocluster/crystal growth. From this we obtain incidental, yet accurate estimates for the silicon surface energy and a Tolman length, $\delta \approx 0.15 \pm 0.1$ nm using the Laplace-Young relation. © 2011 American Institute of Physics. [doi:10.1063/1.3575181]

I. INTRODUCTION

The phonon confinement model (PCM) was initially proposed by Richter *et al.*¹ to describe asymmetrically broadened Raman line shapes from samples containing silicon microcrystals. In single crystal bulk semiconductors the phonon wave-function extends over the entire structure with well defined energy and momentum characteristics. The conservation of momentum for light scattering from phonons means that only those modes at the Brillouin zone (BZ) center (corresponding to a wave-vector, $\mathbf{q}_0 = 0$) are Raman active. In bulk silicon this mode appears at $\omega_{\text{bulk}} = 521 \text{ cm}^{-1}$ with a natural linewidth at room temperature, $\Gamma_0 \sim 4 \text{ cm}^{-1}$. In amorphous material the disrupted translational symmetry and absence of long range order leads to a relaxation of this selection rule and an extension in the number of allowed modes for $\mathbf{q} \neq \mathbf{q}_0$, leading to a broad band of optical phonon spectra, which for SiO_2 is centered around 480 cm^{-1} . The localization of phonons to micro- or nanoscale semiconductor materials (with a small to medium range order and confining length, L) also leads to a relaxation of this selection rule and an uncertainty in the phonon momentum, $\Delta \mathbf{q}$ which increases with the inverse confining length scale, L^{-1} . This gives rise to an increase in the number of Raman active

modes away from the BZ center and results in peak shifts or asymmetrically broadened spectra, the degree of which should be a strong function of the phonon dispersion of the scattering material. The Richter model¹ supposes an infinite crystal wave-function that is weighted by some confinement envelope function, $W(r, L)$ which attenuates its amplitude toward the nanocrystal boundary, i.e., at $2r/L = 1$. The modified Raman line shape may therefore be expressed mathematically as the product of the Lorentzian line-shape function, $L(\omega, q)$, which arises from the inelastic scattering of photons by zone center phonons and the Fourier coefficient of $W(r, L)$, summed over the entire BZ.² A number of models^{1–5}, including that of Richter *et al.*¹ have attempted to determine the phonon confining length scale by fitting the measured Raman spectra under the assumption of a particular boundary value for the phonon wave-function. This approach is unreliable because the boundary value of the phonon wave-function and the confining length scale are mutually dependent. Rather, in this contribution, we invoke the recently adapted PCM of Adu *et al.*⁶ in which we include the measured nanocrystal size and, critically, the distribution of sizes from cross-sectional transmission electron microscopy (X-TEM) images, which defines our phonon confinement length. A general confinement envelope function having Gaussian form can then be employed to fit our measured Raman spectra by optimization of an exponent value, α ,

^{a)}Electronic mail: iain.crowe@.manchester.ac.uk.

which provides the boundary value of the phonon wavefunction. While the results of our investigations concur qualitatively with those in Ref. 6, in that α is found to be independent of the confining length, the actual boundary value we determine differs quantitatively. While the large range of reported values undoubtedly reflect an omission of the size distribution from many models, a more complete comparison should also take into account the fact that the definition of the phonon dispersion characteristics often vary from model to model. In addition to removing anisotropy from the dispersion of bulk optical phonon branches, on account of the random orientation of the nanocrystals, the model should take into account the effects of temperature and pressure on the phonon dispersion. In doing so, we obtain the result that the wave-function probability amplitude is equal to zero only for $2r/L \geq 1$, and thereby remove the rather ambiguous concept of “soft confinement” in which phonons are supposed to “leak” into the surrounding matrix. Furthermore, we are able to infer from our fitting a spectral shift attributable to a difference in pressure across the nanocrystal interface, which is minimized by their growth, analogous to small liquid droplets. Relating the change in pressure to the change in size using the Laplace-Young equation reveals a size-dependent surface energy and an incidental estimate of the Tolman length, both of which are in excellent agreement with literature values.

II. EXPERIMENTAL METHODS

A. Sample preparation

500nm SiO₂ films were grown by “wet” thermal oxidation from either single crystal (100) Si (X-TEM) or sputtered Si on Al₂O₃ (Raman). The oxide films were then implanted with Si⁺ at 80 keV to an areal density of $8 \times 10^{16} \text{ cm}^{-2}$, which yields a distribution of excess Si atoms in a ~ 100 nm wideband, centered ~ 100 nm below the surface, as predicted by Monte Carlo simulations using the Stopping and Range of Ions in Matter (SRIM 2003) and verified by TEM (not shown here). The implanted distribution yields a peak concentration of Si ~ 8 at. % excess, as verified by Rutherford backscattering spectroscopy (RBS) (not shown here). Annealing of the Si supersaturated oxide films to obtain silicon nanocrystals and remove implantation damage was executed using a commercial Jipelec Jetfirst 100 rapid thermal processor in a nitrogen (N₂) ambient for isochronal anneal temperatures in the range 1050 to 1100°C and isothermal anneal times in the range 1 to 600 s. All samples were post-process annealed in a mixed N₂:H₂(5%) forming gas at 500 °C for a further 5 min, which is known to passivate the so-called “dangling-bond” type interfacial defects (P_b -centers).⁷

B. Cross-sectional transmission electron microscopy (X-TEM)

Imaging silicon nanocrystals in SiO₂ is complicated by the similar atomic number and density of the two materials, which gives rise to a low phase contrast.⁸ As such, we adopted a cross-sectional, dark field imaging technique at relatively low magnification first described by Iacona *et al.*⁹

in order to obtain a statistically relevant dataset. Using a Phillips CM-12 TEM at 120 keV, we were able to obtain a large number of silicon nanocrystals (>200) in a single image by aligning the TEM beam along a particular zone axis, in our case <220>. In this way the image contrast is enhanced by the diffraction of the TEM beam electrons from nanocrystal planes aligned along the same axis. While the random orientation of the nanocrystals naturally yields an underestimate for the absolute density using this technique, the relative density, size and distribution of nanocrystals in the implanted layer as a function of annealing time or temperature can be determined in a highly repeatable manner.

C. Raman spectroscopy

The Raman signatures of amorphous and crystalline Si are uniquely distinguishable, which makes this technique particularly suitable to a study of the phase transformation of silicon nanocrystals during annealing. Obtaining Raman spectra from silicon-rich silicon oxide on silicon is problematic however due to the low volume fraction of randomly oriented silicon nanocrystals, the weak signal from which can be swamped by the strong transverse-optical (TO) phonon mode at 521 cm⁻¹ from the substrate. Wellner *et al.*¹⁰ achieved this however for a single layer of silicon nanocrystals in a thin oxide on silicon using a combination of resonant excitation and exploitation of the Raman selection rules. Resonant excitation, for example at 3.4 eV, which corresponds to the direct gap in bulk silicon, greatly enhances the Raman scattering cross section while cross polarizing the exciting and scattered light strongly suppresses the substrate signal relative to that from the nanocrystals because of their random orientation. We were able to avoid such complicated experimental arrangements by studying the Raman spectra from samples prepared via implantation of Si⁺ into SiO₂ on Al₂O₃ (sapphire) substrates and annealed under exactly the same conditions as those studied by X-TEM. Photoluminescence spectra (not shown here) confirmed that these samples exhibited similar optoelectronic properties to those prepared in thermal oxide on silicon.

The samples were excited using the 514 nm line of an Ar⁺ laser focused at the sample using a 50x microscope objective lens. Raman spectra were collected con-focally in a backscattering geometry and dispersed using a Renishaw 1000 micro-Raman system. The signals were detected using a charge coupled device (CCD) camera and the signal to noise ratio was optimized by minimizing the CCD pixel array, increasing the exposure time and averaging accumulated spectra over several minutes. Comparing the spectra with a virgin substrate facilitated removal of the background scattering signal from the sapphire, which is well documented.^{11,12} All measurements were conducted at room temperature.

III. RESULTS AND DISCUSSION

A. Cross sectional dark field transmission electron microscopy (X-TEM)

A selection of X-TEM DF diffraction contrast images for anneal times in the range 1 to 600 s at 1100 °C are shown in Fig. 1.

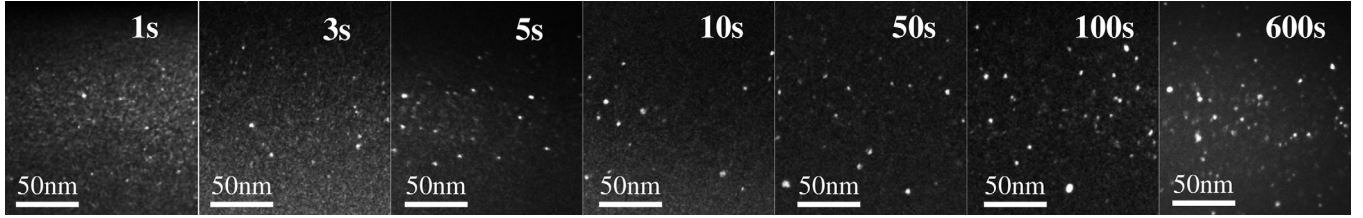


FIG. 1. X-TEM DF diffraction contrast image “atlas” of RTP silicon rich silicon oxide samples on (100) Si. Bright spots are silicon nanocrystals aligned with the <220> zone axis. The programmed annealing time range is 1 to 600 s at 1100 °C and the individual fields of view are 150 nm across × 175 nm high.

The X-TEM image “atlas” of Fig. 1 reveals the effects of isothermal annealing time (t_A) on the silicon nanocrystal size and density. Images to the right (long t_A) reveal large, sparsely populated silicon nanocrystals whereas those on the left (short t_A) are smaller and more populous. In order to obtain a thorough statistical dataset, more than 200 nanocrystals in each image were counted and analyzed to determine their size and density. The uncertainty in determining nanoparticle size using this de-focused imaging technique was previously reported to be around $\pm 5\%$ ^{13,14} and the minimum detectable nanocrystal diameter, which is limited by the resolution of the microscope, is ~ 0.7 nm⁹.

Figure 2 shows representative stack histograms obtained from the X-TEM image “atlas”, which reveal quantitatively the evolution of the silicon nanocrystal size distributions as a function of annealing time.

In agreement with previously reported analyses of the nano-structure size distributions,^{6,15} we find that the histograms in Fig. 2 are most accurately represented by the log-normal PDF, Eq. (1) with characteristic values obtained for the expected (or most probable) nanocrystal size, \bar{L} and standard deviation, σ .

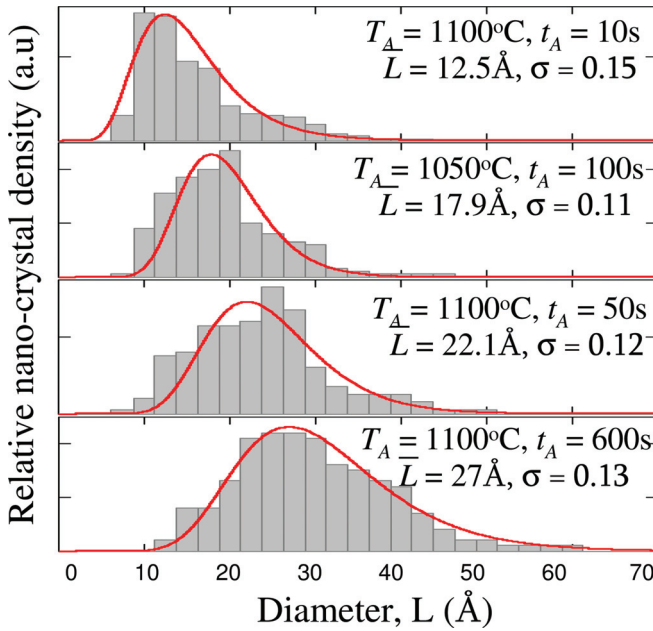


FIG. 2. (Color online) Silicon nanocrystal size distributions as a function of anneal time and temperature (indicated) as determined from the X-TEM image “atlas.” The light gray (red) lines are lognormal fits to the data using Eq. (1) with the characteristic values for the expected diameter, \bar{L} and standard deviation, σ also indicated for each curve.

$$F(L, \bar{L}, \sigma) = \frac{1}{\sigma} \exp \left(-\frac{(\log(L) - \log(\bar{L}))^2}{2\sigma^2} \right). \quad (1)$$

B. Raman spectroscopy and the phonon confinement model (PCM)

In an infinite crystal semiconductor, the phonon wave-function with radial coordinate, r and wave-vector, \mathbf{q}_0 can be written:^{1,2}

$$\Phi(\vec{q}_0, r) = u(\vec{q}_0, r) e^{-i\vec{q}_0 \cdot \vec{r}} \quad (2)$$

where $u(\vec{q}_0, r)$ has the periodicity of the lattice

For the same phonon confined to a spherical nanocrystal, diameter, L we can write the modified wave-function as:

$$\Psi(\vec{q}_0, r) = W(r, L)\Phi(\vec{q}_0, r) = \Psi'(\vec{q}_0, r)u(\vec{q}_0, r) \quad (3)$$

where $W(r, L)$ is defined generally according to:⁶

$$W(r, L) = A e^{(-\alpha r/L)^2} \quad (4)$$

with the wave-function probability amplitude given by:¹

$$|\Psi|^2 = A^2 e^{(-2(\alpha r/L)^2)}. \quad (5)$$

The modified wave-function therefore decays toward the nanocrystal boundary at $2r/L = 1$ with the actual boundary value determined by α .

Expanding $\Psi'(\vec{q}_0, r)$ in a Fourier series provides a means for evaluating the frequency response of the phonon localization, i.e., the effect of localization on the Raman spectrum. A general expression for the Raman line shape, $I(\omega, \mathbf{q})$ is then obtained from the product of the Lorentzian line-shape function, $L(\omega, \mathbf{q})$, which arises from the scattering of light from a dispersion of infinite crystal phonons and the Fourier coefficient of the confinement envelope function, as determined by $C(\vec{q}_0, \vec{q}) \propto \int \Psi'(\vec{q}_0, \vec{r}) e^{-i\vec{q} \cdot \vec{r}} d^3r$ which introduces additional modes for $\mathbf{q} \neq 0$, which is then summed over the entire BZ:

$$I(\omega, \vec{q}) = \int_{BZ} |C(\vec{q}_0, \vec{q})|^2 L(\omega, \vec{q}) d^3q. \quad (6)$$

For 3D confinement, the infinitesimal volume element, d^3q is proportional to ¹⁶ $q^2 dq$ and, considering the Fourier coefficient of the Gaussian confinement envelope function of

Eq. (4),^{1,2} $|C(\vec{q}_0, \vec{q})|^2 = e^{(-q^2 L^2 / 2\alpha^2)}$, we can write a more detailed expression for the Raman line shape as:

$$I(\omega, \vec{q}, L, \alpha) = A \int_0^1 \exp(-q^2 L^2 / 2\alpha^2) \times \left[(\omega - \omega(\vec{q}))^2 + (\Gamma/2)^2 \right]^{-1} q^2 dq \quad (7)$$

where \vec{q} is the reduced wave-vector, having the units of $2\pi/a$ (with $a = 5.43 \text{ \AA}$ being the bulk Si lattice parameter), $\omega(\vec{q})$ is the phonon dispersion and Γ is the linewidth of the spectrum arising from the zone center phonon mode, which includes instrumental broadening,^{6,17} taken to be equal to $\sim 4.7 \text{ cm}^{-1}$.

Equation (7) is the model employed by many authors to fit their measured Raman spectra and in doing so they attempt to access the confining length according to an arbitrary estimate of α , the physical basis for which remains ambiguous. This model however neglects the presence of any size distribution as if sampling a single phonon confinement length, L , i.e., a monodisperse nanostructure size, which is rarely, if ever the case. We prefer to extend this model by incorporating two important features; a parameter which reflects the pressure dependence of the phonon dispersion, which we include by modification of the analytical expression of Eq. (8) after Paillard *et al.*¹⁸

$$\omega(\vec{q}, P) = \sqrt{\omega_0(P)^2 - \frac{A \vec{q}^2}{\vec{q} + 0.53}}. \quad (8)$$

This representation of the phonon dispersion is derived from the Brout sum rule and therefore removes any direction dependence associated with the strong anisotropy of the optical phonons in bulk silicon. This is necessary on account of the fact that the nanocrystals in our samples are randomly orientated as previously verified by TEM¹⁹ (not shown here). In Eq. (8), $A = 1.261 \times 10^5 \text{ cm}^{-2}$ and $\omega_0(P)$ is the sum of the bulk zone center phonon mode frequency, ω_{bulk} ($= 521 \text{ cm}^{-1}$ for Si) and a pressure-dependent shift,²⁰ $\Delta\omega_s$ ($\cong 5P$) with P in GPa, included here as a fitting parameter enabling fine adjustment of the calculated peak position without altering the line shape.

Second, following the method of Adu *et al.*,⁶ we include in our model the measured size distribution (from the X-TEM images) so that the expression for the Raman line shape can be written:

$$I(\omega, \vec{q}, L, \vec{L}, \sigma, \alpha, P) \sim A \int_0^\infty I(\omega, \vec{q}, L, \alpha, P) F(L, \vec{L}, \sigma) dL \quad (9)$$

which is effectively a double integral, one to evaluate the phonon confinement in a single nanostructure, size L for all \vec{q} in the BZ and the other for the diameter distribution including the measured values for \vec{L} and σ , for all L . Since this model removes the size and distribution of sizes as variables, the measured line shape can be fit by adjustment of just three parameters, an amplitude factor, A , which includes the square of the Raman matrix element,⁶ $|M_q|^2$, α , which allows us to determine the actual boundary value of the phonon

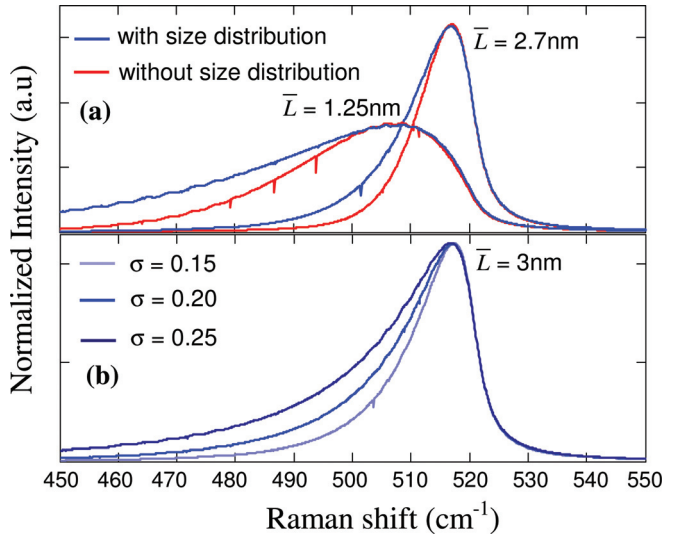


FIG. 3. (Color online) (a) Calculated Raman spectra with [dark gray (blue) line] and without [light gray (red) line] the inclusion of a size distribution for two most probable nanocrystal sizes, $\bar{L} = 2.7 \text{ nm}$ and $\bar{L} = 1.25 \text{ nm}$ [i.e., light gray (red) lines calculated using Eq. (7) and dark gray (blue) lines calculated using Eq. (9) with fixed α and P]. (b) Calculated Raman spectra [Eq. (9)] with increasing size distribution, σ for a fixed $\bar{L} = 3 \text{ nm}$.

wave-function and P , which provides quantitative data on the film stress according to the absolute spectral shift, relative to that predicted by the PCM.

Figure 3 illustrates the effect of size distribution on the Raman line shape, underpinning the importance of its inclusion in the model.

The presence of a size distribution increases the asymmetry of the spectra to lower frequencies, the degree of which increases monotonically with increasing size distribution without shifting the peak position. This indicates that the peak position is a strong function of the most probable nanocrystal size, \bar{L} . On the other hand, Fig. 4 illustrates the effect on the Raman spectra for increasing the fitting parameters, α and P , highlighting their competitive nature in determining the final peak position and width.

Figure 5 shows our measured spectra obtained after excitation using the 514 nm line of an Ar⁺ laser as well as the fits using Eq. (9) all as a function of the annealing conditions.

Figure 5 indicates a complex spectral shape, which is distinguishable from the background between 450 and 540

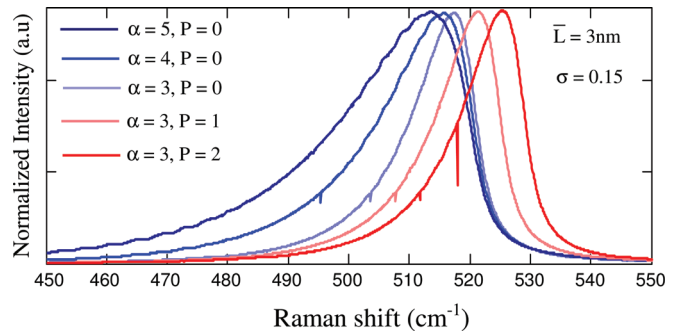


FIG. 4. (Color online) Calculated Raman spectra using Eq. (9) for a distribution of silicon nanocrystals with most probable nanocrystal size, $\bar{L} = 3 \text{ nm}$ and $\sigma = 0.15$. Dark gray (blue) lines indicate increasing values for α with fixed $P (= 0)$ and the light gray (red) lines indicate increasing values for P with fixed $\alpha (= 3)$.

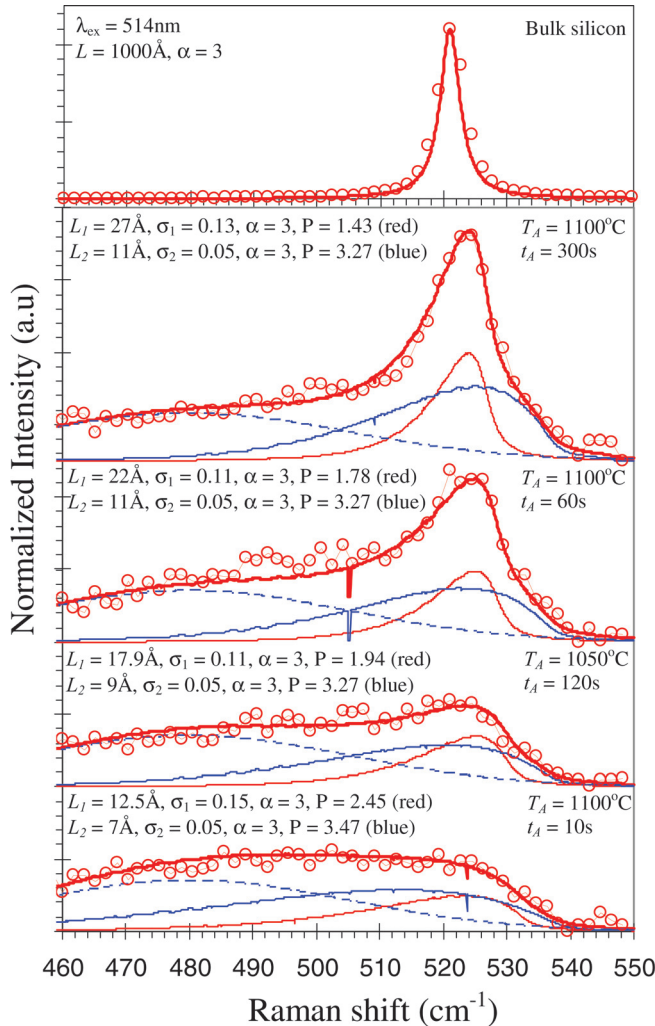


FIG. 5. (Color online) Thermal evolution of the measured (circles) Raman spectra (offset for clarity) and corresponding fits for the measured (X-TEM) silicon nanocrystal size distributions [thin light grey (red) line] and the high frequency background scattering spectrum from ultrasmall silicon nanocrystals [dark gray (blue) line] using Eq. (9). The convolution [bold light gray (red) line] was obtained by the inclusion of a constant (Gaussian) scattering contribution with a peak at 480 cm^{-1} , which arises from the a-SiO₂ films [dashed dark gray (blue) line]. At the very top of the figure is a measured (circles) bulk silicon reference spectrum which is fit using Eq. (7) for comparison.

cm^{-1} . A broad, featureless band centered around 500 cm^{-1} is evident even after just 10 s of annealing at 1100°C . This band falls away sharply above 530 cm^{-1} and, as the annealing time is increased a sharper feature emerges around 525 cm^{-1} . It is noteworthy that the spectrum from the sample annealed for 120 s at the lower temperature of 1050°C is only marginally more intense than that annealed for just 10 s at 1100°C , yet significantly weaker than that annealed for 60 s at 1100°C . This indicates the much stronger dependence of silicon nanocrystal formation on T_A than on t_A in agreement with the TEM data and previously reported observations.²¹

A number of interesting observations emerge from the fits; the first and most apparent being that the fits corresponding to the measured (X-TEM) size distributions (in Fig. 5) are insufficient alone in describing the high frequency spectral components. In fact, a second fit (in Fig. 5) was required to describe the background scattering spectrum, which adds

significant contributions to the Raman spectra at lower frequencies as well as a shoulder at higher frequencies. In order to model these contributions we have had to assume that α , which we have determined to have a value of three for all fits corresponding to the measured size distributions, is independent of the confining length, in qualitative agreement with Adu *et al.*⁶ Then, we have fit this high frequency background scattering spectrum by optimization of \bar{L} , σ , and P with the results indicating that the likely source of the background scattering spectra is a secondary population of ultra-small (sub-nm), amorphous silicon nanoclusters that are invisible in the X-TEM images. Indeed, bimodal size distributions were already reported for Raman analyses of amorphous nanocrystalline Si (Refs. 22 and 23) and porous Si (Ref. 24) thin films.

We would like to make a comment about estimating the crystalline fraction (of nanoclusters), ρ_c from Raman scattering spectra. We note that such estimates were previously obtained using Eq. (10):^{25–27}

$$\rho_c = \frac{I_c}{(I_c + yI_a)} \quad (10)$$

where I_c and I_a are the integrated intensities of the respective crystalline and amorphous contributions to the total Raman scattering spectrum and y is supposed to be the ratio of crystalline to amorphous scattering cross sections. It was reported by Bustarret *et al.*²⁸ that y exhibits a size dependence according to $y(L) = y(\infty) + e^{-L/250}$ with $y(\infty)^{26,28} = 0.1$. However, the very presence of a bimodal cluster population, each of which has a wide size and therefore scattering cross-section distribution as well as contributions from the SiO₂ to the final spectrum calls into question the accuracy of this approach. We are of the opinion that, without the support of at least one other analytical technique, an unambiguous determination of the absolute crystalline fraction cannot be justified.²⁹ Rather, an estimate of the relative increase in crystalline fraction, x is more appropriate when considering the thermal evolution of the Raman scattering spectra alone. We obtained such a value from our empirical convoluted peak sum fit (in Fig. 5), which we calculated using Eq. (11):

$$I_{\text{peaksum}} = A[xp_1 + (1 - x)p_2] + Bp_3 \quad (11)$$

with p_1 and p_2 , respectively, representing the crystalline and amorphous nanocluster scattering peaks and $B (= 0.07)$ representing a constant intensity of the scattering peak, p_3 associated with the a-SiO₂ film. The magnitude of the fitting parameters, A and x increased from 1.5 to 2.5 and 0.4 to 0.65, respectively with increasing thermal budget which we believe reflects both an increased contribution from the nanoclusters (crystalline and amorphous) to the total scattering spectrum as well as a relative increase in their crystalline fraction.

Next we address the physical interpretation of α , the size of which determines the boundary value of the phonon wave-function as shown in Fig. 6 for a range of reported values⁶ and that determined in this work.

It is tempting to conclude that the wide range of reported α -values⁶ is a result of the sensitivity of the Raman scattering to the nanostructure surface phonon modes. Indeed, this interpretation was eluded to already by a number of investigators^{30,31} in what is typically referred to as “soft confinement,” whereby the phonon effectively “leaks” out into the surrounding matrix. However, most workers^{2,3,6,16,17,32,33} report better agreement with their measured data, either by increasing α or by defining the confinement envelope to be a sinc function,^{18,34} analogous to the ground state electronic wave-function in an infinite potential well, both of which yield a boundary value of zero for the phonon wave-function. The difference being that the latter ensures that the value of the phonon wave-function goes to zero only at the nanocrystal boundary, which, with the exception of the shape of the wave-function inside the nanocluster amounts to a similar result as that we have obtained in this work, where $\alpha = 3$. We note that when employing the general Gaussian confinement envelope function of Eq. (4), values of $\alpha > 3$ leads to decay of the phonon wave-function to values much closer to zero well within the boundary, i.e., for $2r/L < 1$, for which there appears to be no physical justification, despite the multiplicity of reports.^{2,3,6,17,32} While the large range of reported values undoubtedly reflects an omission of the size distribution from many models, a more complete comparison should also take into account the fact that the definition of the phonon dispersion characteristics often varies from model to model.^{5,6,18,31} In addition to removing anisotropy from the dispersion of bulk optical phonon branches, on account of the random orientation of the nanocrystals, the model should take into account, where relevant, the effects of temperature^{3,17} and pressure^{25,35} on the phonon dispersion characteristics. In doing so, we obtain the result that the wave-function probability amplitude is equal to zero only for $2r/L \geq 1$, which removes the unnecessary and rather ambiguous concept of “soft confinement.”

Finally we examine the pressure parameter, P , which we note from our fitting increases monotonically with the inverse thermal budget (and therefore inverse nanocrystal size). We interpret this in the following way; Anomalous up-shifted Raman peaks were already reported and attributed

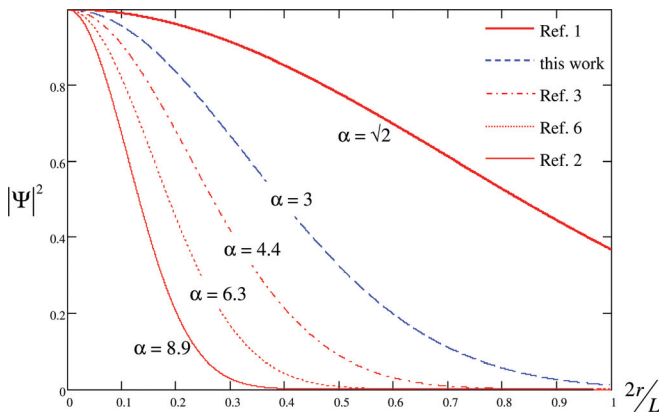


FIG. 6. (Color online) Effect of α -value on the modified phonon wave-function confined within a nanocrystal, size L (i.e., for $2r/L \leq 1$).

to compressive stress^{36,37} or hydrostatic pressure,²⁵ which acts in opposition to the effect of phonon confinement with the competition between the two effects determining the observed (measured) peak position. A similar qualitative result was previously reported by Hernandez *et al.*²⁵ In that work the authors attributed the stress to an abrupt lattice mismatch between the matrix and the surface of the nanocrystals. The authors of Ref. 25 proposed that the smaller values determined for larger silicon nanocrystals could be due to a combination of smaller surface to volume ratio and the presence of a pressure relieving amorphous shell which separates their crystalline core from the surrounding matrix. We adopt a more fundamental approach and assume that the nanocrystals/clusters behave like small spherical liquid droplets where the pressure difference across their interface is minimized by their growth (stress relaxation), with a corresponding change in their surface energy. For example, if, during the relaxation process, the pressure difference across the interface of a spherical nanocrystal, $p_i - p_o = P$ results in an increase in the particle radius from r to $r + dr$, then there is “work done” equivalent to the product $PAdr$. The equivalent change in surface energy is then given by $dE = \gamma dA$, where γ is the surface tension and dA is the corresponding change in surface area. Equating the “work done” to the change in surface energy then yields the well known Laplace–Young relation given by Eq. (12):

$$P = \frac{2\gamma}{r} = \frac{4\gamma}{L} \quad (12)$$

using the values of L and P from our measurements and fitting we determine that the surface energy, γ exhibits a size dependence as shown in Fig. 7.

In fact the size dependence of the surface tension was already reported for a range of materials^{38–41} confirming that it

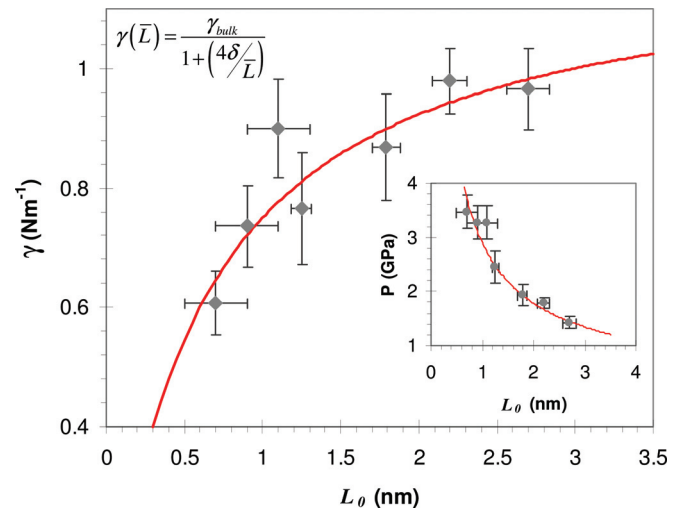


FIG. 7. (Color online) Surface energy (filled diamonds) as a function of most probable silicon nanocrystal/cluster size. The bold gray (red) line is a fit to the measured data using the generalized size-dependent surface energy relation (Refs. 38–41) [Eq. (13)]. With $\gamma_{bulk} \approx 1.2 \text{ Nm}^{-1}$, Tolman length, $\delta \approx 0.15 \text{ nm}$. The inset shows the estimated pressure (circles) as a function of the nanocrystal/cluster size as determined from the spectral fitting parameter, P . The size of the error bars are derived from the confidence of the fits in Fig. 5 based on an optimized coefficient of determination (R^2 -value).

is a general property of nano-particles. The values we calculated for γ increase from ~ 0.6 to $\sim 1 \text{ Nm}^{-1}$ when the expected particle size, \bar{L} increases from ~ 0.7 to $\sim 2.7 \text{ nm}$. Despite the apparent mixed phase nature of the silicon nanoclusters in our samples and the fact that the reported values for the surface energy of amorphous silicon are typically lower than those for crystalline silicon, the wide range of values reported for the bulk surface energy,^{42–45} in our view, justifies the single fit to the data in Fig. 7 assuming a straightforward capillary approach in accordance with the approximate but adequately precise Tolman relation,⁴⁶ Eq. (13):^{38–41}

$$\gamma(\bar{L}) = \frac{\lambda_{\text{bulk}}}{1 + (4\delta/\bar{L})}. \quad (13)$$

Obtaining an accurate value for the Tolman length, δ then naturally depends on the correct choice for the bulk surface energy, γ_{bulk} . We used an average experimental value for the planar bulk silicon surface energy⁴⁵, $\gamma_{\text{bulk}} (\approx 1.2 \text{ Nm}^{-1})$ to retrieve an estimate of the Tolman length, $\delta (\approx 0.15 \pm 0.1 \text{ nm})$, which appears to be in reasonable agreement with those in the literature Ref. 41.

It is worthy of note however that, for the special case of crystalline nanoparticles, an interphase (or mixed phase) transition region, which separates the crystalline core of ultrasmall particles from their surrounding host matrix^{25,46} likely determines the surface tension probed in this work (and possibly in many other works). Of course, the presence of such an interface region might explain why the size effect of the surface tension appears to dominate any obvious phase dependency, although one cannot rule out other factors that are known to affect the surface energy, such as surface oxidation^{47,48} or hydrogenation.⁴⁴

IV. CONCLUSIONS

We studied the Raman spectra corresponding to the Si TO phonon mode around 520 cm^{-1} as a function of the annealing environment for Si^+ implanted, thermally grown oxide films on Al_2O_3 (sapphire) substrates. The monotonic increase in the peak around 520 cm^{-1} evidences the presence of Si–Si bonds and the formation of crystalline particles with increasing long range order. This is consistent with the formation and growth of silicon nanocrystals with increasing thermal budget. In order to explain the peak shift and asymmetric broadening relative to that from single crystal bulk silicon we fitted the measured Raman spectra with a modified PCM based on that originally developed by Richter *et al.*¹ The degree of phonon confinement is expected to be a strong function of the nanocrystal size and since the total Raman spectrum represents a superposition of allowed optical modes, the line shape should therefore depend on the specific size distribution being sampled. Based on X-TEM image analysis of silicon nanocrystals prepared in a similar manner, we reveal that this size distribution is most accurately represented by the lognormal PDF. Invoking the PCM recently adapted by Adu *et al.*,⁶ which includes this measured size distribution gives physical meaning to our model and critically removes uncertainty in determining the con-

finement length scale. By defining the Gaussian confinement envelope function generally and including an analytical phonon dispersion, which removes the direction dependence associated with optical phonons in bulk silicon, we obtain excellent fits to the normalized measured Raman spectra by optimization of just two fitting parameters, α and P . The former determines the exponent value of the confinement function providing the actual boundary value of the phonon wave-function and the latter, which is included in the analytical expression for the phonon dispersion provides quantitative information about stress in the films. The fits to our measured Raman spectra indicate that there is a bi-modal population of nano-structures with similar size distributions, although only one of which, exhibiting some crystalline fraction, is visible in the X-TEM images. The model indicates that the second population, which is inferred from the high frequency background scattering spectrum, are extremely small (sub-nm), amorphous nanoclusters. Bi-modal size distributions were also reported previously for nc-Si formed in $a\text{-SiO}$ matrices via laser annealing⁵ and more recently in Si/SiO_2 multilayer structures prepared by magnetron sputtering.⁴⁹

We were able to fit all of our measured Raman spectra under the assumption of a constant α -value, indicating that the boundary value of the phonon wave-function is independent of the confinement length, in qualitative agreement with Adu *et al.*⁶ Critically, the α -value we obtain specifically implies rigid confinement with the wave-function probability amplitude approaching zero only for $2r/L \geq 1$. We postulate that inconsistent definitions for the phonon dispersion may be, in part responsible for the range of reported α -values.

Finally, our fitting parameter P , which has the effect of shifting the spectra to higher frequencies and therefore competes with the effect of phonon confinement, indicates the presence of stress in the films, which turns out to be a strong function of the most probable nanocluster size. Using the values we obtained for this stress induced Raman shift, in conjunction with the Laplace-Young relation, we determined values for the size-dependent surface tension and the Tolman length, which appear to be in good agreement with the literature values.⁴¹

ACKNOWLEDGMENTS

This work was funded by the Engineering and Physical Sciences Research Council (UK).

- ¹H. Richter, Z. P. Wang, and L. Ley, *Solid State Commun.* **39**, 625 (1981).
- ²I. H. Campbell and P. M. Fauchet, *Solid State Commun.* **58**, 739 (1986).
- ³P. Mishra and K. P. Jain, *Phys. Rev. B* **62**, 14790 (2000).
- ⁴P. Mishra and K. P. Jain, *Phys. Rev. B* **64**, 073304 (2001).
- ⁵M. C. Rossi, S. Salvatori, F. Galluzzi, and G. Conte, Mater. Sci. Eng. B **69–70**, 299 (2000).
- ⁶K. W. Adu, H. R. Gutiérrez, U. J. Kim, G. U. Sumanasekera, and P. C. Eklund, *Nano Lett.* **5**, 409 (2005).
- ⁷P. Pellegrino, B. Garrido, C. García, R. Ferré, J. A. Moreno, and J. R. Morante, *Physica E (Amsterdam)* **16**, 424 (2003).
- ⁸B. G. Fernandez, M. Lopez, C. Garcia, A. Perez-Rodriguez, J. R. Morante, C. Bonafos, M. Carrada, and A. Claverie, *J. Appl. Phys.* **91**, 798 (2002).
- ⁹F. Iacona, G. Franzo, and C. Spinella, *J. Appl. Phys.* **87**, 1295 (2000).
- ¹⁰A. Wellner, V. Paillard, H. Coffin, N. Cherkashin, and C. Bonafos, *J. Appl. Phys.* **96**, 2403 (2004).

- ¹¹M. Kadlecovábaé, J. Breza, and M. Veselý, *Microelectron. J.* **32**, 955 (2001).
- ¹²R. N. Favors, Y. Jiang, Y. L. Loethen, and D. Ben-Amotz, *Rev. Sci. Instrum.* **76**, 033108 (2005).
- ¹³C. Bonafos, B. Garrido, M. Lopez, A. Perez-Rodriguez, J. R. Morante, Y. Kihn, G. Ben Assayag, and A. Claverie, *Mater. Sci. Eng. B* **69–70**, 380 (2000).
- ¹⁴C. Bonafos, D. Mathiot, and A. Claverie, *J. Appl. Phys.* **83**, 3008 (1998).
- ¹⁵V. A. Belyakov, V. A. Burdov, R. Lockwood, and A. Meldrum, *Adv. Opt. Technol.* **2008**, 279502 (2008).
- ¹⁶M. Grujic-Brojcin, M. J. Scepanovic, Z. D. Dohcevic-Mitrovic, and Z. V. Popovic, *Acta Phys. Pol. A* **116** (2009).
- ¹⁷K. W. Adu, H. R. Gutierrez, U. J. Kim, and P. C. Eklund, *Phys. Rev. B* **73**, 155333 (2006).
- ¹⁸V. Paillard, P. Puech, M. A. Laguna, R. Carles, B. Kohn, and F. Huisken, *J. Appl. Phys.* **86**, 1921 (1999).
- ¹⁹R. J. Kashtiban, U. Bangert, I. F. Crowe, M. P. Halsall, B. Sherliker, A. J. Harvey, J. Eccles, A. P. Knights, R. M. Gwilliam, and M. Gass, *Journal of Physics: Conference Series* (Iop, Oxford, UK, 2010), Vol. 209.
- ²⁰S. Bhattacharyya, D. Churochkin, and R. M. Erasmus, *Appl. Phys. Lett.* **97**, 141912 (2010).
- ²¹C. Bonafos, B. Colombeau, A. Altibelli, M. Carrada, G. Ben Assayag, B. Garrido, M. López, A. Pérez-Rodrígues, J. R. Morante, and A. Claverie, *Nucl. Instrum. Methods in Phys. Res.* **178**, 17 (2001).
- ²²D. Gracin, A. Gajovic, K. Juraic, M. Ceh, Z. Remes, A. Poruba, and M. Vanecek, *J. Non-Cryst. Solids* **354**, 2286 (2008).
- ²³S. K. Ram, M. N. Islam, P. Roca i Cabarrocas, and S. Kumar, *Thin Solid Films* **516**, 6863 (2008).
- ²⁴M. N. Islam and S. Kumar, *Appl. Phys. Lett.* **78**, 715 (2001).
- ²⁵S. Hernandez, A. Martinez, P. Pellegrino, Y. Lebour, B. Garrido, E. Jordana, and J. M. Fedeli, *J. Appl. Phys.* **104**, 044304 (2008).
- ²⁶R. Tsu, J. Gonzalez-Hernandez, S. S. Chao, S. C. Lee, and K. Tanaka, *Appl. Phys. Lett.* **40**, 534 (1982).
- ²⁷S. B. Concari and R. H. Buitrago, *Semicond. Sci. Technol.* **18**, 864 (2003).
- ²⁸E. Bustarret, M. A. Hachicha, and M. Brunel, *Appl. Phys. Lett.* **52**, 1675 (1988).
- ²⁹C. Ossadnik, S. Veprek, and I. Gregora, *Thin Solid Films* **337**, 148 (1999).
- ³⁰S. Bhattacharyya and S. Samui, *Appl. Phys. Lett.* **84**, 1564 (2004).
- ³¹V. Tripathi, M. Nazrul Islam, Y. N. Mohapatra, and P. Roca i Cabarrocas, *Eur. Phys. J.: Appl. Phys.* **39**, 203 (2007).
- ³²Y. Kanemitsu, H. Uto, Y. Masumoto, T. Matsumoto, T. Futagi, and H. Mimura, *Phys. Rev. B* **48**, 2827 (1993).
- ³³S. K. Gupta and P. K. Jha, *Solid State Commun.* **149**, 1989 (2009).
- ³⁴H. Münder, C. Andrzejak, M. G. Berger, U. Klemradt, H. Lüth, R. Herino, and M. Ligeon, *Thin Solid Films* **221**, 27 (1992).
- ³⁵H. Hofmeister, F. Huisken, and B. Kohn, *The Eur. Phys. J. D* **9**, 137 (1999).
- ³⁶S. Yerci, U. Serincan, and I. Dogan, *J. Appl. Phys.* **100**, 074301 (2006).
- ³⁷G. Viera, S. Huet, and L. Boufendi, *J. Appl. Phys.* **90**, 4175 (2001).
- ³⁸R. C. Tolman, *J. Chem. Phys.* **17** (1949).
- ³⁹D. Mukherjee, A. Prakash, and M. R. Zachariah, *Aerosol Sci.* **37**, 1388 (2006).
- ⁴⁰H. M. Lu and Q. Jiang, *Langmuir* **21**, 779 (2004).
- ⁴¹H. M. Lu, *Solid State Phenom.* 155 (2009).
- ⁴²R. J. Jaccodine, *J. Electrochem. Soc.* **110**, 524 (1963).
- ⁴³S. Hara, S. Izumi, T. Kumagai, and S. Sakai, *Surf. Sci.* **585**, 17 (2005).
- ⁴⁴T. Hawa and M. R. Zachariah, *J. Chem. Phys.* **121**, 9043 (2004).
- ⁴⁵M. Legros, G. Dehm, E. Arzt, and T. J. Balk, *Science* **319**, 1646 (2008).
- ⁴⁶B. Kidyarov, *J. Struct. Chem.* **45**, S31 (2004).
- ⁴⁷Z. F. Yuan, K. Mukai, and W. L. Huang, *Langmuir* **18**, 2054 (2002).
- ⁴⁸X. Huang, S. Togawa, S.-I. Chung, K. Terashima, and S. Kimura, *J. Cryst. Growth* **156**, 52 (1995).
- ⁴⁹V. Osinniy, S. Lysgaard, V. Kolkovsky, V. Pankratov, and A. N. Larsen, *Nanotechnology* **20**, 195201 (2009).